Conf-750915--14

deHAAS-vanALPHEN EFFECT IN URh_3 AND UIr_3

by

A. J. Arko, M. B. Brodsky, G. W. Crabtree,
D. Karim, L. R. Windmiller & J. B. Ketterson

For Presentation at
5th International Conference on Plutonium and Other Actinides
Baden-Baden, Germany
September 9-13, 1975

U of C-AUA-USERDA
ARGONNE NATIONAL LABORATORY, ARGONNE, ILLINOIS

operated under contract W-31-109-Eng-38 for the
U. S. ENERGY RESEARCH AND DEVELOPMENT ADMINISTRATION

deHAAS-vanALPHEN EFFECT IN URh_3 AND UIr_3*

A. J. Arko, M. B. Brodsky, G. W. Crabtree
D. Karim, L. R. Windmiller,
Argonne National Laboratory
Argonne, Illinois 60439 USA

and

J. B. Ketterson
Northwestern University
Evanston, Illinois

and

Argonne National Laboratory
Argonne, Illinois 60439 USA

July 1975

To be presented at the 5th International Conference on Plutonium and Other Actinides, Baden-Baden, Germany, September 9-13, 1975.

*Work supported by the U. S. Energy Research and Development Administration.

DEHAAS-VANALPHEN EFFECT IN URh_3 AND UIr_3*

A. J. Arko, M. B. Brodsky, G. W. Crabtree,
D. Karim, L. R. Windmiller,
Argonne National Laboratory
Argonne, Illinois 60439 USA

and

J. B. Ketterson
Northwestern University
Evanston, Illinois 60201 USA
and
Argonne National Laboratory
Argonne, Illinois 60439 USA

ABSTRACT

Measurements of the deHaas-vanAlphen effect have been performed in the intermetallic compounds URh_3 and UIr_3. Complex spectra are observed in both materials. Effective mass measurements were made for several orbits in URh_3 and values as large as 5.3 m_o were observed. The relatively complete data in URh_3 are consistent with a complex multiply-connected Fermi surface which is in qualitative agreement with band structure calculations. The largest frequency branches in UIr_3 appear to have the same topology as their corresponding branches in URh_3. In addition, a number of closed low-mass surfaces exist in UIr_3 and are discussed in terms of the calculations for URh_3.

I. INTRODUCTION

Measurements of the deHaas-vanAlphen (dHvA) effect, which can yield precise information about electronic bands at the Fermi level and are traditionally used as a Fermi surface probe, have been utilized to study the band structure of the intermetallic compounds URh_3 and UIr_3. Qualitative agreement is observed with band structure calculations [1] at least in URh_3 where both calculations and data are more complete.

Few complete band structure calculations have been made for actinide materials in the past not only because of the difficulties in the calculations (e.g., low-symmetry crystal structures, large numbers of conduction electrons per unit cell, need for relativistic calculations, etc.) but also because of the lack of precise and detailed experimental data with which to compare such calculations [2]. DeHaas-vanAlphen (dHvA) measurements suffer from the requirement of nearly perfect single crystals, which because of phase transitions and chemical reactivity are extremely difficult to obtain in the actinide metals. While detailed measurements exist for thorium metal [3,4], only scant data are available for uranium where it is necessary to do the measurements at pressures above 8.3 Kbar in order to suppress the low-temperature phase transitions [5]. No dHvA data exist for metals beyond uranium, and the prospects for obtaining them are not encouraging at this point. In these materials the effective masses (see following section) for f-like bands are likely to be very large so that the dHvA amplitudes are probably diminished beyond the sensitivity of presently available equipment. Also, it is not yet clear whether the f-electrons can always be treated within the band picture.

The severe experimental difficulties encountered in the actinide metals are reduced in actinide intermetallic compounds, in some cases to the point where the

*Work supported by the U. S. Energy Research and Development Administration.

dHvA effect can be observed. Thus, our attention has been focussed on compounds. The spectrum of f-electron properties obtained in the compounds is even richer than for the pure metals which makes this an exciting field of study.

The compounds reported in this paper (URh_3 and UIr_3) have bulk properties similar to relatively simple transition metals although it was proposed from other investigations [6] that at least in URh_3 broadened, itinerant f-states do exist at the Fermi level. Both materials have a temperature-independent susceptibility while the low-temperature resistivities vary as T^3 for URh_3 and as T^5 for UIr_3 [7]. It is apparent that these compounds do not have local moment properties found in many actinide intermetallics especially those with the $AuCu_3$ structure [8]. However, it is this lack of narrow bands or localized 5f levels which is in itself interesting. On the empirical plots representing the correlation between actinide-actinide separation and magnetic or superconducting properties [9], both URh_3 and UIr_3 fall well into the region that should be magnetic (lattice constants for the ordered $AuCu_3$-type structure are 3.991 Å and 4.023 Å, respectively). It will be shown that the lack of magnetism can be attributed to the formation of hybridized d-f bands.

Investigations of compounds displaying narrow-band phenomena (e.g., UGe_3) [10] such as spin fluctuations have been initiated and show a wealth of dHvA oscillations. However, the requirements of sample purity are much more severe in these materials where effective masses are very large. Somewhat purer specimens than those presently available (Dingle temperature $\approx$4°K, see below) are needed in order to investigate the entire Fermi surface. These materials will constitute the basis for future study.

The data for URh_3 presented in this paper are fairly complete so that a Fermi surface model can be constructed. The measurements on UIr_3 need to be done at higher fields to clear up some details. Nevertheless, a fairly clear picture is emerging even for UIr_3. In Section II we give a brief description of the dHvA effect together with the method of measurement. Sample preparation is discussed in Section III, while results and discussions of both compounds are presented in Section IV. Conclusions are drawn in Section V.

II. dHvA EFFECT - THEORY AND MEASUREMENT

Since numerous review articles exist on this subject [11] no attempt will be made to discuss the effect in detail. However, some pertinent equations will be presented together with some of the more important definitions.

The dHvA effect, or the oscillatory diamagnetic susceptibility, results from the quantization of free electron orbits in a plane normal to a magnetic field H. The quantum condition is given as

$$\Phi = (n + \gamma)2\pi\hbar c/e \tag{1}$$

where Φ is the magnetic flux through an area encircled by an electron orbit, n is an integer, γ is a phase factor, $\hbar$ is Planck's constant, and e the electronic charge. The cross-sectional areas of allowed orbits in real space then are given by $(n + \gamma)2\pi\hbar c/eH$, while in k-space, through Onsagers relations, the allowed areas are give by [12]

$$A_n = (n + \gamma)2\pi eH/\hbar c. \tag{2}$$

The electrons in these orbits are separated in energy E by an amount $\Delta E = \hbar eH/m^*$ where m^* is the so-called cyclotron-effective mass of the electrons. It is defined as

$$m^*(E,\hat{\varepsilon}) = \frac{\hbar^2}{2\pi}\left(\frac{\partial A}{\partial E}\right)_{\hat{\varepsilon}}. \tag{3}$$

Here $\hat{\varepsilon}$ is a unit vector along the magnetic field direction.

Clearly as H increases, both the area of the n^{th} orbit in k-space and the energy of the electrons in the n^{th} allowed orbit increase until at a sufficiently high value of H the area just equals the cross-sectional area of the Fermi surface, A_F, and the energy equals the Fermi energy, E_F. Increasing H still further causes a depopulation of the electrons from the n^{th} orbit to orbits with lower energy since the electrons cannot have an energy larger than E_F. The $(n-1)^{th}$ orbit now becomes the highest occupied orbit. This depopulation causes a small oscillation in the free energy, magnetization, density of states, and other related properties. It occurs regularly in intervals proportional to 1/H with frequency

$$F = \hbar c A_F / 2\pi e \tag{4}$$

so that the magnetization oscillates periodically in 1/H. Onsager has shown [12] that oscillations are obtained only from those portions of the Fermi surface where the cross-sectional areas in the plane normal to the magnetic field have an extremum. On all other portions the variation of A_F causes such rapid changes in frequency that phase cancellation occurs, smearing out the oscillations.

For the general case where the Fermi surface has i extremal areas, the magnetic field and temperature dependence of this oscillatory magnetization is given approximately by:

$$\vec{M}(H,\hat{\varepsilon},T) = \sum_i \vec{B}_i(H,\hat{\varepsilon},T)\sin\left[\frac{2\pi F_i(\hat{\varepsilon})}{H} + \beta_i(\hat{\varepsilon})\right] \tag{5a}$$

$$\vec{B}_i(H,\hat{\varepsilon},T) = \frac{\hat{C}_i(\hat{\varepsilon})H^{-1/2}\tau\cos[\pi g_i m_i^*(\hat{\varepsilon})/2m_o]}{\sinh[2\pi^2 kc(T + X_i(\hat{\varepsilon}))m_i^*(\hat{\varepsilon})/\hbar eH]} \tag{5b}$$

where $\vec{M}$ is the magnetization, $\vec{B}_i$ and β_i are the amplitude and phase, respectively, of the quantum oscillation of frequency $F_i(\hat{\varepsilon})$ [given in Eq. (4) above] for a given temperature T, magnetic field strength H, and field orientation $\hat{\varepsilon}$ with respect to crystallographic axes. The Zeeman splitting factor also can vary for each sheet of Fermi surface and is given by g_i. $\hat{C}_i(\hat{\varepsilon})$ is a quantity determined by the geometry of the Fermi surface in the immediate neighborhood of the i^{th} extremal plane, while the effective temperature term, $X_i(\hat{\varepsilon})$, which accounts for the existence of a finite electron scattering time, is directly related to crystal imperfections, and is referred to as the Dingle temperature.

The Fermi surface of most metals is quite complex consisting of several distinct sections or sheets supporting many different extremal cross-sectional areas for a given magnetic field direction $\hat{\varepsilon}$. The areas can differ in size from only a few tenths of a percent of one another to as much as four orders of magnitude. The situation is further complicated since the amplitudes of the different dHvA frequency components can differ by many orders of magnitude.

Thus, in determining the Fermi surface of metals using the dHvA effect, the basic experimental problem is the spectrum analysis of Eq. (5a) into each of its components $F_i(\hat{\varepsilon})$, or through Eq. (4), into $A_i(\hat{\varepsilon})$. (In our discussion we will use the words frequency or area interchangeably.) One then plots $A_i(\hat{\varepsilon})$ versus $\hat{\varepsilon}$ to obtain the angular variation of the areas. Looking at Eq. (5b) one sees that the amplitude of oscillations is enhanced if $X_i(\hat{\varepsilon})$ and T are very small, and if H is large. Thus, it becomes necessary to use very pure and perfect single crystals ($X_i(\hat{\varepsilon}) < 1°K$) and to work at very low temperatures. We performed our experiments at temperatures below 0.4°K using ^3He evaporative cooling and at fields as large as 132 kG using a Nb_3Sn superconducting solenoid. The largest field used thus far for UIr_3 was only 70 kG. A rotating probe was used to orient the crystal in the magnetic field (i.e., change $\hat{\varepsilon}$). The usual field-modulation technique was used to obtain dHvA signals [13]. In this technique the sample is placed in a

pickup coil and the magnetization is measured as a voltage induced in the pickup coil. A small modulating field $\{h \cos(\omega t)\}$ is superimposed on the d.c. field H, and the pickup voltage is usually phase-detected at 2ω or 3ω in order to eliminate the voltage picked up directly from the modulating field. The spectral content of the dHvA signal (the pickup coil voltage vs 1/H) was analyzed by an on-line PDP-11/20 mini-computer programmed to perform fast or slow Fourier transforms [14]; this latter capability proves absolutely essential when analyzing complex dHvA spectra.

A second important quantity one measures with the dHvA effect is $m_i^*(\hat{\varepsilon})$. Essentially it is a measure of how tightly bound the conduction electron is to the nuclear site, or put in different terms, how broad or narrow the bands are at the Fermi energy. In URh_3 we measured masses as large as 5.3 m_o where m_o is the rest mass of a free electron. This is an extremely large quantity when compared to masses as low as 0.01 m_o in some simple metals. The mass is obtained by measuring the quantity $B_i(\hat{\varepsilon})$ vs T. A plot of $\ln(B_i(\hat{\varepsilon})/T)$ vs T yields a straight line, the slope of which is proportional to $m_i^*(\hat{\varepsilon})$.

Another measureable quantity $X_i(\hat{\varepsilon})$, or the Dingle temperature, was not investigated in detail. However, Dingle temperatures $\approx$0.5K were measured in URh_3 and somewhat lower values found in UIr_3. The spin splitting factor g_i also was not investigated although from the URh_3 data it was apparent that it was probably considerably larger than the free electron value of 2.

III. SAMPLE PREPARATION

A variety of methods are being used to grow single crystals of actinide compounds. The purest crystals are produced in an electron beam floating zone furnace; however, its use is restricted to materials with the proper characteristics. In the case of URh_3 and UIr_3 both are congruent-melting line compounds and the vapor pressures of the constituent metals at the melting temperature of the compounds are sufficiently low that melting in a vacuum causes no variations in sample stoichiometry. Consequently, the floating zone technique was used here. The compounds were initially prepared by rf heating of the constituent metals in a water-cooled silver boat in an inert atmosphere using 5N rhodium, 6N iridium, and 4N uranium. A rod of each specimen ($\approx$5 cm long x $\approx$3 mm diameter) was then electron-beam zone refined in vacuum three times to form the crystal and purify the rod. In this manner crystals of URh_3 and UIr_3 were obtained having residual resistance ratios of 170 and 285, respectively. For dHvA measurements a small crystal ($\approx$0.8 mm on each side) was electrolytically cut from each of the large rods and etched to remove cutting damage.

A number of other crystals have also been grown by different techniques. Crystals of UGe_3 and USi_3 were grown by dissolving the material in a Bi flux and slowly lowering the temperature from $\approx$900°C. USn_3 was grown by simply dissolving a small amount of U in Sn and again lowering the temperature slowly from $\approx$900°C. This technique is useful where vapor pressure or transformation problems preclude the use of the floating zone. For compounds where one or both of the constituents has a high vapor pressure but otherwise melts congruently above $\approx$1200°C, the Czochralsky method, using a tri-arc furnace and an intert atmosphere, may prove most effective.

IV. RESULTS AND DISCUSSION

A. URh_3

Figures 1 and 2 show the extremal cross-sectional area $A_i(\hat{\varepsilon})$, in atomic units, measured in URh_3 as a function of magnet angle in the (100)- and (110)-type crystallographic planes. The measured effective masses are given in Table 1.

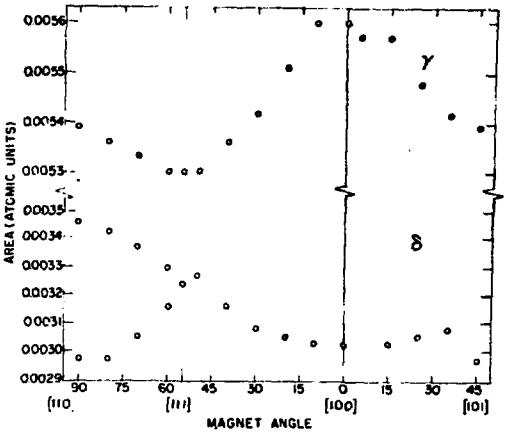

Fig. 1. Cross-sectional areas in atomic units for the small, closed surfaces in URh_3 in the (100) and (110) planes. Because of the very low anisotropy the various branches of δ could not be clearly resolved.

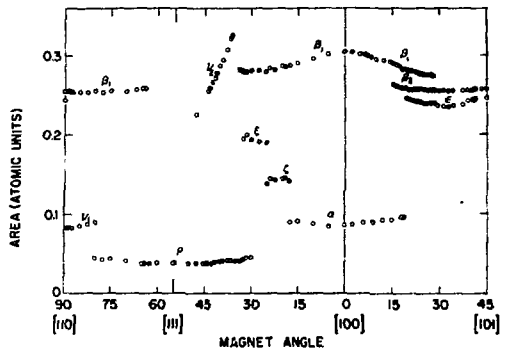

Fig. 2. Cross-sectional areas in atomic units for the large, open piece of Fermi surface in URh_3 in the (100) and (110) planes.

TABLE I

EFFECTIVE MASSES IN URh_3

Orbit	Plane	Degrees from [100]	Effective Mass, m^*/m_o
α	(100)	0°	2.50
γ	"	0°	0.49
δ	"	0°	0.61
β_1	"	0°	3.01
"	"	12.5°	3.16
"	"	18.5°	3.30
"	"	24.5°	3.70
β_2	"	18.5°	5.12
"	"	24.5°	4.03
"	"	30.0°	3.88
"	"	34.5°	3.71
"	"	45.0°	3.73
ε	"	34.5°	3.66
ρ	(110)	70.0°	2.35
"	"	54.5°	2.22
"	"	33.0°	3.00
β_1	"	80.0°	3.80
"	"	70.0°	5.00
"	"	65.0°	5.25
"	"	28.0°	4.01

Most of the frequencies are very disjointed (primarily in Fig. 2) indicating a complex, multiply-connected Fermi surface. Only the very small frequencies in Fig. 1 come from closed surfaces. The frequency branch labeled γ can be identified with a surface located either at Γ or at R (see Fig. 3 for symmetry labels in the simple cubic Brillouin zone) while the set of frequencies labeled δ are probably due to a set of closed surfaces somewhere along the Γ-X line. From Table I one sees that these small surfaces have very low effective masses (0.4 m_o-0.6 m_o) and probably have considerable s-wave character. However, they represent only a very small fraction of the total Fermi surface.

The bulk of the Fermi surface is identified with the data of Fig. 2. Effective masses ranging from 2.5 m_o to 5.3 m_o have been measured for the various extremal orbits. Electron masses on the branches ν_1, ζ, and ξ are probably higher than 5.3 m_o but could not be measured since the appropriate oscillations were observable only at the lowest temperatures. It is believed that all of these frequency branches are related and come from one multiply-connected Fermi surface.

The large slowly varying branches β_1 appear to be due to a set of ellipsoids connected to each other via necks which cause the observed interruptions in the extremal orbits. The branch ν_1 is most likely the neck frequency so that from the [110] minimum in extremal area we infer that the neck directions are along [110]. The symmetry of the ellipsoids cannot be determined from the data alone. However, band structure calculations (shown in Fig. 4) indicate that the largest piece of Fermi surface is centered at M [1]. By centering the ellipsoids at the points M in the simple cubic Brillouin zone, and connecting them by [110]-directed necks, we obtain a Fermi surface topologically similar to that shown in Fig. 3. Here we have placed spheroids rather then ellipsoids at M since we do not yet know the Fermi surface in such detail; also, we have not included the small, closed surfaces. There are three inequivalent ellipsoids in the zone (labeled 1, 2, and 3 in Fig. 3) filling up about 1/2 the zone volume.

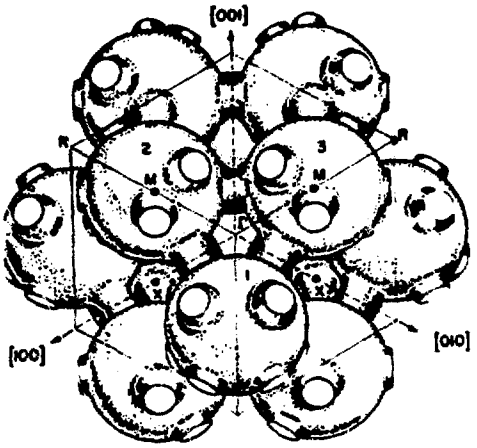

Fig. 3. Symmetry labels and proposed topology for the large, open surface in URh_3. We have shown spheres instead of ellipsoids centered at M and connected by [110]-directed necks.

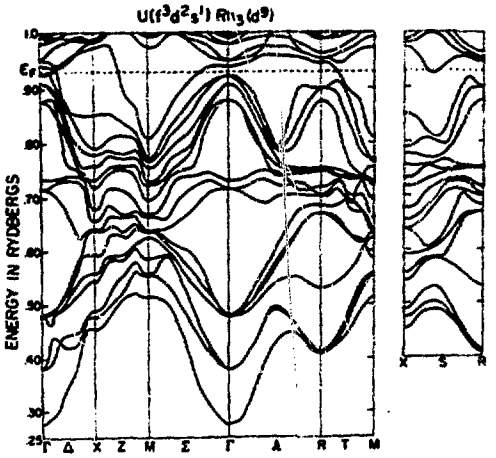

Fig. 4. Energy bands (from Ref. 1) for URh_3 using the electron potential which resulted in a best fit to the data. Note the wide intersection with the Fermi energy around the M-point and also the small intersection identified as a neck along the X-R line.

The calculated bands shown in Fig. 4 are in qualitative agreement with the Fermi surface proposed above. By placing the Fermi energy at 0.93 Ry., we obtain a large surface centered at M of approximately the correct magnitude to correspond to the β_1 orbit. The same band which intersects E_F around M, also intersects E_F along the X-R line and produces the [110]-directed necks. Several small intersections also occur along the Γ-X line which could correspond to the orbits γ and δ in Fig. 1. The orbit γ, however, definitely has the symmetry of either Γ or R and this is not obtained from the bands in Fig. 4. However, these small intersections are extremely sensitive to the s-electron content of the electron potential [1] so that only slight modifications are probably necessary to yield better results along the Γ-X line.

Most of the data in Fig. 2 can be explained on the basis of a Fermi surface having the topology shown in Fig. 3. Frequency branches β_i are entirely consistent with M-centered ellipsoids whose surfaces are interrupted by [110]-directed necks. Frequency branches ν_1 and ν_2 are essentially the neck orbit interrupted for a range of angles where another neck interferes with a closed electron path. The frequency branch ρ comes from a hole orbit centered along the Γ-R line for H along [111] and encompasses three ellipsoids and the three necks connecting them. Frequency branch α is most likely the R-centered hole orbit for H along [100] which includes four ellipsoids and four necks connecting them. Although discontinuous jumps in the four-fold R-centered orbit are possible as H is tipped from [100] in the (110) plane, the most likely explanation for frequency branches ζ and ξ are corrugations in either the necks or ellipsoids or both. Thus, we believe that ζ and ξ are merely continuations of α.

There are some discrepancies between the data and the model of the Fermi surface in Fig. 3. 1) A second hole orbit centered at X should exist for H along [100] and is not observed. 2) Frequency branch ν_1, identified as the neck orbit, is not observed directly at [110] and in the entire (100) plane. 3) Three ellipsoid branches β_i should exist in the (100) plane, each over a limited range of angles. While three branches are actually observed we are reluctant to identify the branch labeled ϵ with β_3 since with the assumed topology it cannot exist at [110]. A data point was obtained at [110] with a value roughly corresponding to ϵ.

Objections 1) and 2) above can be dismissed relatively easily by assuming a high effective mass. This is a reasonable assumption since we know that the mass on the neck orbit is too large to measure even where it is observable. The third problem however presents a greater challenge. There are several possibilities, all of which will require a more complete band structure calculation for resolution. The most likely explanation is that the branch ϵ can indeed be identified as β_3 and it disappears $\gtrsim 5°$ from [110]. The point observed directly at [110] is related to ν_1 in an unknown way, possibly through an additional unobserved piece of Fermi surface.

B. UIr_3

The data for UIr_3 are not yet as complete as for URh_3. Data were taken only in fields up to 70 kG. No effective mass measurements have been made, although it appears from the generally larger signals that the masses are somewhat lower than in URh_3.

The cross-sectional areas obtained in UIr_3 are shown in Fig. 5. Although the details of the connectivity of some branches will need to be cleared up at high fields, a fairly clear picture is nevertheless emerging. A first glance at the data indicates a considerably more complex Fermi surface than in URh_3. However, a closer scrutiny reveals that the band structure is probably quite similar to URh_3, except for a slight downward shift in the Fermi energy.

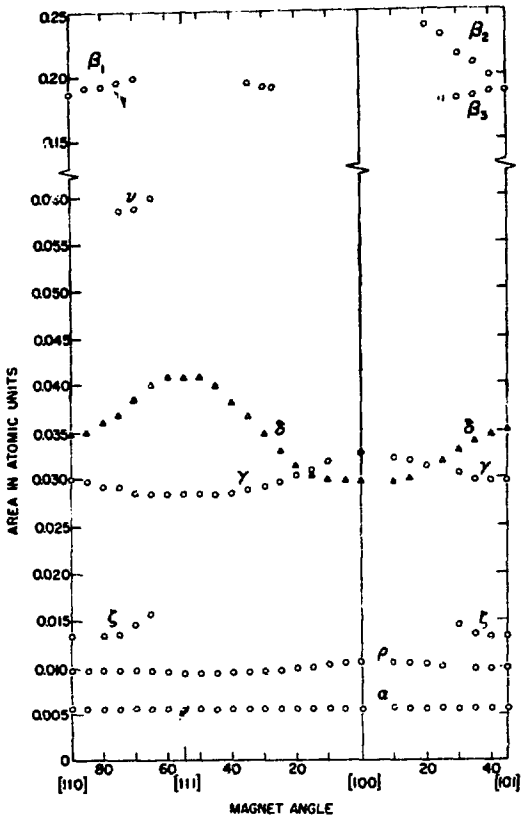

Fig. 5. Cross-sectional areas in atomic units for UIr_3 in the (100) and (110) planes. The branches β_i probably come from a large open piece of Fermi surface. The branch ν may be a neck frequency. Additional branches exist but could not be clearly resolved at 70 kG.

The largest frequencies (labeled β_i in Fig. 5) are about 25% smaller than the corresponding β_i frequencies in URh_3. The symmetry is again consistent (though not conclusively so) with ellipsoids located at M and connected by [110]-directed necks. For example, a single frequency is observed in the (110) plane while multiple frequencies exist in the (100) plane. The orbit in the (110) plane is also interrupted for H near [111] as in URh_3. Unfortunately, the signal slowly fades out within ≈20° of [100] in all planes probably because the effective mass is increasing. It is essential that data be taken at higher fields to clear up the details around [100], and thus firmly establish the symmetry of this surface.

A few additional details also need clearing up. We have not, for example, found a frequency branch which can be clearly identified with a neck orbit. It too is expected to have a large effective mass. The branch labeled ζ is reminiscent of a neck orbit but is probably too small to fit our proposed model. The branch labeled ν is of correct magnitude but has been observed over too small an angular range to make any identification. This too must be remeasured at higher fields. In any case, it appears that the major piece of Fermi surface is probably similar to that shown in Fig. 3.

The remaining four branches are relatively straightforward. They all have the symmetry of either Γ or R and can be identified with single closed surfaces. Except for the branch δ they appear to be octahedrons with the peaks along [100]-type directions. A fifth branch (not shown in Fig. 5) was observed near 0.045 a.u. but could not be clearly resolved at 70 kG. If one looks at the band structure in Fig. 4 one sees that by lowering the Fermi energy to about 0.90 Rydbergs one obtains from four to six additional hole pockets depending on the exact location of E_F, together with a decrease in the size of the electron surface at M. Roughly that is what is observed. It is also necessary for the band which gives rise to the neck to drop down in energy somewhat along the X-R line relative to other bands in order to intersect E_F. Preliminary calculations by Koelling [15] indicate that this indeed appears to be the case in UIr_3. Thus, we feel that even with incomplete data the Fermi surface of UIr_3 is qualitatively understood with a number of details still to be clarified.

V. CONCLUSIONS

Although the band structure calculations for actinide compounds are not yet at a level where one can compare minute details of theory and experiment, the qualitative agreement reported here is certainly encouraging. On the basis of these results one can understand the breakdown of the empirical correlation of actinide-actinide separation and magnetism [9]. Despite the presence of three f-electrons in occupied bands in URh_3 and UIr_3, none of the bands at the Fermi level (see Fig. 4) can be described as very flat or narrow, a description generally associated with f-bands. The broadening of the bands is due to f-d hybridization which is very favorable in the $AuCu_3$ crystal structure, the d-electrons being supplied by the Rh and Ir atoms. The actinide-actinide separation is probably more significant with respect to magnetism in those compounds where the d- or s-electrons responsible for hybridization and broadening of the bands are contributed by the actinde atoms themselves.

The T^3 resistivity in URh_3 is easily understood from the band structure of Fig. 4 and is attributed to interband scattering from the small low mass s-like sheets to the heavy-mass f-d surface [16]. In UIr_3, on the other hand, we have considerably more low-mass pieces of Fermi surface so that a scattering event does not necessarily remove an electron from the current beam. The conduction electrons have a high probability of being scattered into another low-mass band. Hence, we observe a T^5 resistivity at low temperatures, typical of s-s scattering. Indeed it is gratifying to note that the model derived earlier to explain the bulk property data for these compounds [6] is essentially corroborated by the present detailed measurements.

The next step in the investigation of actinide intermetallic compounds is the study of materials displaying nearly-magnetic phenomena such as spin fluctuations. UGe_3 has been mentioned above, and is the most likely candidate if samples with Dingle temperatures of 1°K or less can be obtained. However, some Laves-phase materials such as UIr_2 may prove more fruitful in future studies since higher purities are possible. Clearly, a continued close collaboration between theory and experiment will be necessary for further understanding of these relatively complex materials.

REFERENCES

1. A. J. Arko, M. B. Brodsky, G. W. Crabtree, D. Karim, D. D. Koelling, L. R. Windmiller and J. B. Ketterson, to be published; D. D. Koelling and A. J. Freeman, this conference.

2. An excellent review of the electronic structure of the actinides can be found in: The Actinides: Electronic Structure and Related Properties, A. J. Freeman and J. B. Darby, Jr., eds., Academic Press, New York, 1974.

3. R. P. Gupta and T. L. Loucks, Phys. Rev. B3, (1971) 1834.

4. D. J. Boyle and A. V. Gold, Phys. Rev. Letters 22, (1969) 461.

5. J. E. Schirber, A. J. Arko and E. S. Fischer, Solid State Comm., to be published.

6. M. B. Brodsky, A. J. Arko, A. R. Harvey, and W. J. Nellis, The Actinides: Electronic Structure and Related Properties, Vol. II, A. J. Freeman and J. B. Darby, Jr., eds., Academic Press, New York, 1974, pp. 185-264; W. J. Nellis, A. R. Harvey, and M. B. Brodsky, AIP Conf. Proc. 10, (1973) 1067; A. J. Arko, R. J. Trainor, M. B. Brodsky, G. P. Sykora and W. J. Nellis, to be published.

7. M. B. Brodsky and A. J. Arko, to be published.

8. D. J. Lam and A. T. Aldred, The Actinides: Electronic Structure and Related Properties, Vol. I, A. J. Freeman and J. B. Darby, Jr., eds., Academic Press, New York, 1974, pp. 109-179; W. J. Nellis and M. B. Brodsky, The Actinides: Electronic Structure and Related Properties, Vol. II, 1974, pp. 265-288.

9. H. H. Hill, Plutonium 1970 and Other Actinides, W. N. Miner, ed., Nucl Met. 17, (1970) 2.

10. K. H. J. Buschow and H. J. vanDaal, AIP Conf. Proc. No. 5, Magnetism and Magnetic Materials-1971, C. D. Graham and J. J. Rhine, eds., AIP, New York, Pt. 2, 1464-1477.

11. See for example A. V. Gold in Solid State Physics: The Simon Fraser University Lectures, Vol. I, J. F. Cochran and R. R. Haering, eds., Gordon and Breach, New York, 1968, and references therein.

12. L. Onsager, Phil. Mag. 43, (1952) 1006.

13. For full details of measurement see L. R. Windmiller and J. B. Ketterson, Rev. Sci. Inst. 39, (1968) 1672.

14. L. R. Windmiller, J. B. Ketterson, and J. C. Shaw, ANL-7907, available through the National Technical Information Service, U. S. Department of Commerce, (1972).

15. D. D. Koelling, private communication.

16. A. H. Wilson, Proc. Roy. Soc. London A167, (1938) 580.